

Numerical Methods for the Calculation of Material Parameter Values for Trilayered Porcine Aortic Valve Leaflets

Abstract

Porcine aortic valve leaflets are comprised of three layers, each of which has a different composition and consequently, different mechanical properties. Each layer exhibits non-linear stress-strain behaviour and is modelled using a hyperelastic material model. Our objective is to determine the mechanical properties of each layer from experimental force-indentation depth data, ensuring that the material model parameters in each layer are unique and have converged to their correct values. To achieve this objective, material model parameters are calculated using inverse finite element simulations and non-linear optimization methods. To ensure that these parameters converge to their correct values, mathematical models of the indentation problem are used to obtain approximate values of these parameters to be used as initial conditions in the finite element simulations. This paper describes our progress with the development of these mathematical models and numerical simulations, as well as our ongoing work to achieve our defined objective.

Keywords

aortic valve — finite element method — hyperelastic material — indentation — inverse problem — material parameter estimates — micromechanical properties

Matthew G. DOYLE, Department of Mechanical and Industrial Engineering, University of Toronto, mg.doyle@utoronto.ca

Tracy L. STEPIEN, Department of Mathematics, University of Pittsburgh, tls52@pitt.edu

Pak-Wing FOK, Department of Mathematical Sciences, University of Delaware, pakwing@udel.edu

Huaxiong HUANG, Department of Mathematics and Statistics, York University, hhuang@yorku.ca

Greg LEWIS, Faculty of Science, University of Ontario Institute of Technology, greg.lewis@uoit.ca

Sivalal SIVALOGANATHAN, Department of Applied Mathematics, University of Waterloo, ssivalog@math.uwaterloo.ca

Rebecca VANDIVER, Department of Mathematics, St. Olaf College, vandiver@stolaf.edu

Craig A. SIMMONS, Department of Mechanical and Industrial Engineering, University of Toronto, c.simmons@utoronto.ca

Introduction

Calcific aortic valve disease (CAVD) is the most common disease of heart valves, affecting 25% of the population over the age of 65 years [1]. It is a progressive disease, in which the aortic valve leaflets stiffen and eventually calcify. Currently, there is no medical treatment for this disease and when leaflets become severely calcified, valve replacement is the only treatment. The progression of CAVD in the early stages is not well understood, particularly at the cellular level. It has previously been shown [2, 3] that cells in the valve leaflets, known as valve interstitial cells, differentiate to pathological cell types in response to changes in their mechanical environment and this cell differentiation contributes to the progression of CAVD. Furthermore, the cells sense these changes in their mechanical environment at the microscale. It is therefore essential that more detailed information be obtained concerning the microscale mechanical properties of the extracellular matrix (ECM) surrounding valve interstitial cells in leaflets in both healthy and pathological states.

Porcine aortic valve leaflets, considered in this study, are used in the Simmons Cellular Mechanobiology Laboratory as models for human leaflets because they are similar in size, have similar structure, and display similar structural and cellular changes during early disease [4]. The leaflets are made up of three layers, which are, from the aorta side to the left ventricle side, the fibrosa, the spongiosa, and the ventricularis. Each of these layers has a different ECM composition, with the fibrosa being a collagen-rich layer, the spongiosa being a proteoglycan-rich layer, and the ventricularis containing collagen and elastin. Differences in ECM composition lead to differences in mechanical properties, with the fibrosa being the stiffest layer, followed by the ventricularis, and the spongiosa [5, 6]. Further, the leaflet layers are heterogeneous, with a strong spatial variation in their mechanical properties, and the microscale mechanical properties of the fibrosa and ventricularis layers are nonlinear [6].

The objective of this study is to determine the local microscale mechanical properties of each of the porcine aortic valve leaflet layers from experimental data obtained from intact excised leaflets. To achieve this objective, an inverse finite element

approach is used in conjunction with non-linear optimization. With a single set of force-displacement data per measurement location, the inverse problem is ill-posed for a multilayer material. To address this issue, mathematical models are used to approximate the material parameter values, and these approximations are used as initial conditions for the finite element simulations to ensure that the simulations converge to a solution that is both unique and correct. Work on these mathematical models began in July 2012 at the MBI Math Biosciences Problem-Solving Workshop [7] and the work presented in this paper is the result of ongoing collaborations amongst several of the participants from this workshop.

1. Methods

This project is divided into four main parts: indentation experiments, ultrasound imaging, mathematical models, and numerical simulations. Figure 1 is a flow chart illustrating the workflow for the overall project. Because the focus of this paper is on the mathematical and numerical parts of this study, the first two parts, indentation experiments and ultrasound imaging, are only briefly described in the following sections.

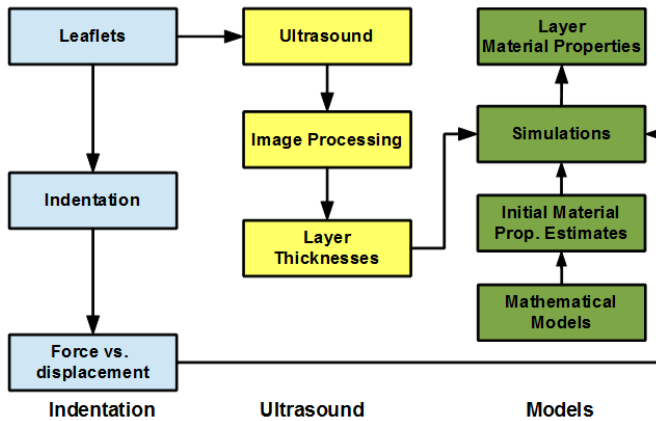


Figure 1. Project workflow diagram

1.1 Indentation experiments

Porcine hearts were obtained from a local abattoir (Quality Meat Packers, Ltd., Toronto, ON, Canada). Aortic valve leaflets were isolated and pinned to a silicone substrate, which was embedded in a Petri dish. The leaflets were covered with a small amount of phosphate buffered saline (PBS) and placed on a sample stage for indentation. A purpose-built microindenter was used to indent the leaflets with a cylindrical indenter tip having a diameter in the range of 50-150 μm . Figure 2 is a schematic of the leaflet-indenter system. Indentation forces and the corresponding indentation depths were measured using this system. The measured indentation depths were used as input boundary conditions in the numerical simulations. An example of an indentation force versus indentation depth data for two locations on each of two leaflets is shown in Figure 3.

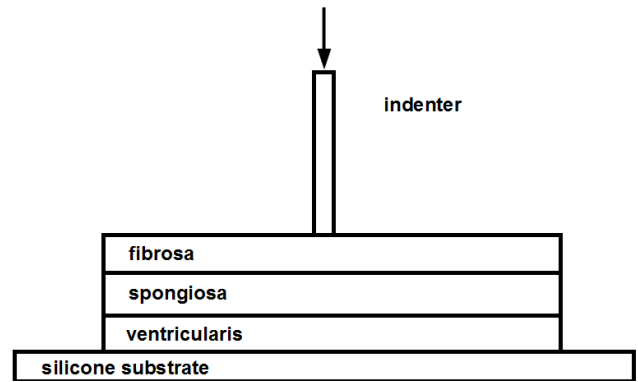


Figure 2. Schematic of leaflet indentation

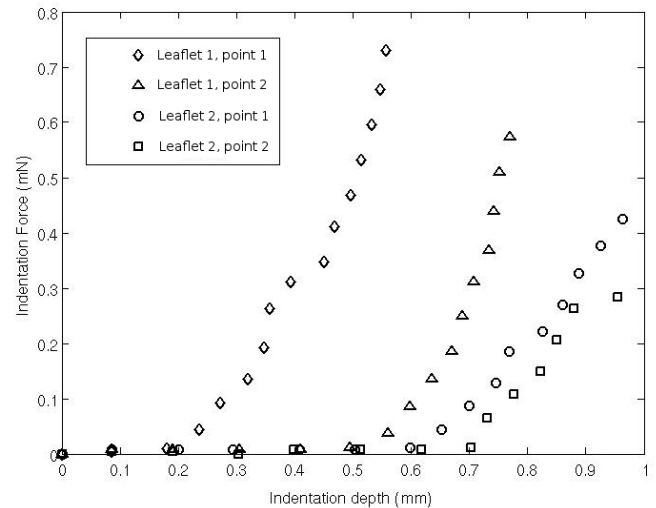


Figure 3. Typical indentation force versus depth curves

1.2 Ultrasound

Following a method proposed by Qiu et al. [8], a pre-clinical ultrasound system (Vevo 770; Visualsonics, Inc., Toronto, ON, Canada) was used to obtain B-mode ultrasound images of the aortic valve leaflets. These images, such as the one shown in Figure 4, show a cross-sectional view of the leaflet, including the three layers. Using image processing functions in MATLAB (The MathWorks, Inc., Natick, MA, USA), these images were filtered and segmented. The thicknesses of the layers were then calculated from the segmented images and these thicknesses were used to define the geometry in the numerical simulations.

1.3 Material models

Nonlinear stress-strain (or force-displacement) data can be modelled by a hyperelastic material model, defined by a strain energy density function W . In this study, we have chosen an exponential form of W , which has previously been used to model soft tissues, including aortic valve leaflets [9]. The incompressible form of this material model is defined as

$$W = \frac{C_1}{2} \left(e^{C_2(I_1-3)} - 1 \right), \quad (1)$$

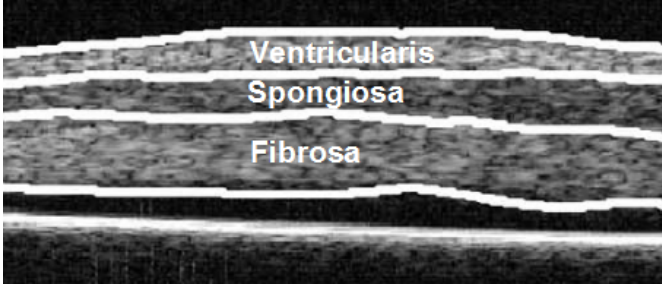


Figure 4. Segmented B-mode ultrasound image of the three aortic valve leaflet layers

where C_1 and C_2 are material parameter values, $I_1 = \sum_i \lambda_i^2$ is the first invariant of Green's strain tensor, $\lambda_i = l_i/l_{i,0}$ are the principle stretches, l_i is the material length, and $l_{i,0}$ is the undeformed material length.

1.4 Mathematical models

Mathematical models are used to estimate the material properties of the leaflet layers from the experimental data, and these estimated properties are used as initial conditions in the inverse finite element simulations. This section describes the formulations of these models. To simplify the models considerably, contact effects between the indenter and the leaflet have been neglected.

1.4.1 One-dimensional model

Starting from Equation (1), we consider a special case where the only non-zero stress is in the $x = x_1$ direction. In this case, we have $\lambda_2 = \lambda_3$, and assuming incompressibility, we have

$$\lambda_2 = \lambda_3 = \frac{1}{\sqrt{\lambda_1}}. \quad (2)$$

The strain energy density function is now written as

$$W = \frac{C_1}{2} \left(e^{C_2(\lambda_1^2 + 2\lambda_1^{-1} - 3)} - 1 \right). \quad (3)$$

The stress in the x direction can be obtained as

$$\sigma = -p + \lambda_1 \frac{\partial W}{\partial \lambda_1} = -p + C_1 C_2 (\lambda_1^2 - \lambda_1^{-1}) e^{C_2(\lambda_1^2 + 2\lambda_1^{-1} - 3)}, \quad (4)$$

where p is the hydrostatic pressure.

1.4.2 One-layer problem

Let us consider a single leaflet layer of thickness h , where $x = 0$ is the bottom surface, and $x = h$ is where the force F (per unit area) is applied. From the equilibrium condition $\partial \sigma / \partial x = 0$, we have

$$-p + C_1 C_2 (\lambda^2 - \lambda^{-1}) e^{C_2(\lambda^2 + 2\lambda^{-1} - 3)} = F. \quad (5)$$

To simplify notation, we have dropped the subscript for λ_1 . The value of p depends on the side boundary condition and for simplicity we assume that $p = 0$. Equation (5) indicates that for a given force, the stretch is a constant.

Equivalently, for a given indentation depth U , we can compute the stretch $\lambda = (h - U)/h$. From Equation (5), we can compute the force F . If we have a pair of indentation depth-force values $U(1)/F(1)$ and $U(2)/F(2)$, we can easily back out the material parameters C_1 and C_2 by solving for C_2 first from the ratio $F(1)/F(2)$. Figure 5 is a plot of a force-indentation depth curve for this one-layer model.

Finally, we note that if we take a third pair of measurement $U(3)/F(3)$, we can use it to find the thickness h . However, we cannot do it using the simple approach outlined above. Instead, we need to solve a coupled system of nonlinear equations for C_1 , C_2 , and h .

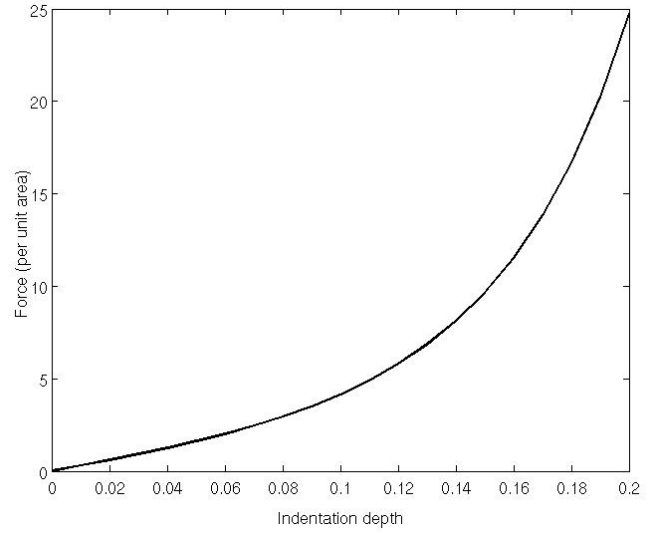


Figure 5. Force-indentation depth curve for Equation (5) with $h = 1$, $C_1 = 1$, and $C_2 = 10$. The symbols are the sample values that were used to estimate the value for C_2

1.4.3 Two-layer problem

Let us now consider two layers with different material parameters C_{i1} and C_{i2} ($i = 1, 2$) and thicknesses h_1 and h_2 , as shown in Figure 6. Because stress is the same in each layer, we have

$$F = -p_1 + C_{11} C_{12} (\lambda_1^2 - \lambda_1^{-1}) e^{C_{12}(\lambda_1^2 + 2\lambda_1^{-1} - 3)} \quad (6)$$

$$= -p_2 + C_{21} C_{22} (\lambda_2^2 - \lambda_2^{-1}) e^{C_{22}(\lambda_2^2 + 2\lambda_2^{-1} - 3)}. \quad (7)$$

For a fixed force F , Equations (6) and (7) indicate that both stretches λ_i ($i = 1, 2$) are constants. **Note that the subscript for λ is now used to represent the different layers.**

At the bottom $x = 0$, we have $u_1(0) = 0$; on the interface between two layers $x = h_1$, we have $u_1(h_1) = u_2(h_1)$; and at the top $x = h_1 + h_2$, we have $u_2(h_1 + h_2) = U$, where u_1 and u_2 are the displacements in layers 1 and 2, respectively and U is the indentation depth. The stretches are

$$\lambda_1 = 1 - \frac{u_1(h_1)}{h_1}, \quad (8)$$

$$\lambda_2 = 1 - \frac{U - u_1(h_1)}{h_2} = 1 + \frac{h_1}{h_2} - \frac{U}{h_2} - \frac{h_1}{h_2} \lambda_1. \quad (9)$$

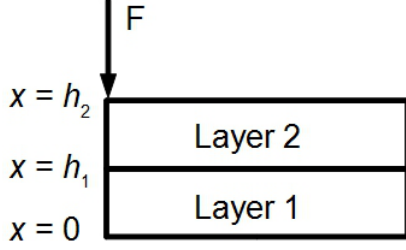


Figure 6. Diagram of two-layer problem

For simplicity, we assume that the far field side conditions are such that $p_1 = p_2 = 0$. For each force F , we have three equations

$$h_1\lambda_1 + h_2\lambda_2 = h_1 + h_2 - U \quad (10)$$

and

$$F = C_{11}C_{12}R(\lambda_1)e^{C_{12}S(\lambda_1)} \quad (11)$$

$$= C_{21}C_{22}R(\lambda_2)e^{C_{22}S(\lambda_2)}. \quad (12)$$

To simplify notation, we have used

$$R(\lambda) = \lambda^2 - \lambda^{-1}, \quad S(\lambda) = \lambda^2 + 2\lambda^{-1} - 3.$$

In Figure 7, we have plotted the force- λ curve to illustrate the nonlinear behaviour.

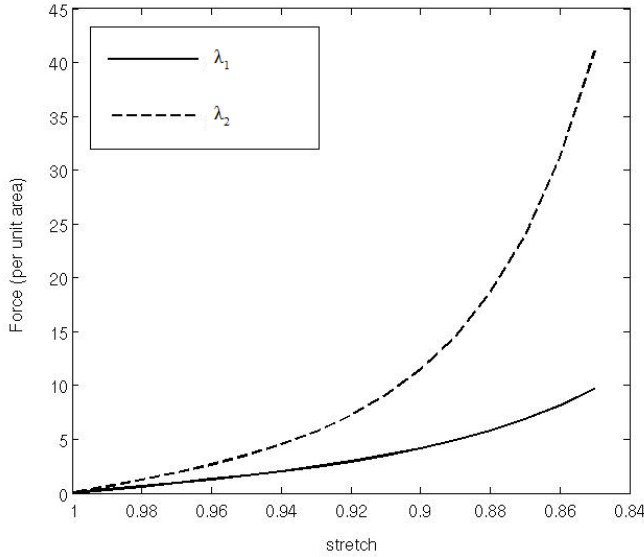


Figure 7. Force- λ curve for Equation (12) with $h_1 = h_2 = 1$, $C_{11} = C_{21} = 1$, $C_{12} = 10$, and $C_{22} = 2C_{12}$

In general, the procedure for finding the material parameter values is more complicated for multilayer problems. When deformation is small, $\lambda = 1 + \delta$ with $\delta \ll 1$. In this case, $R(\lambda) \sim \delta + \delta^3$ and $S(\lambda) \sim 2\delta^2$, from which we have $R(\lambda) \exp(C_2 S(\lambda)) \sim \delta + (1 + 2C_2)\delta^3$. Thus, depending on relative sizes of δ and C_2 , we might have a linear or cubic nonlinearity as two special

cases. In Section 2.1, we will use these two special cases to illustrate the non-uniqueness for the linear case and a solution procedure for the cubic nonlinear case.

1.4.4 Two-dimensional model

The one-dimensional model described in the previous section provides some useful information. However, its ability to accurately predict the material parameters is limited, so we consider a model that will be used to provide reasonable approximations, while being less computationally expensive than the ANSYS finite-element model discussed in detail in Section 1.5. The goal is to use this simpler model to obtain good first estimates of the material parameters, which will ultimately enable faster convergence of the optimization process when using the more physically accurate material model (Equation 1). The results from this model will also provide a means of verifying the results of the ANSYS simulations.

For a general strain energy density function $W = W(\mathbf{F})$, where \mathbf{F} is the deformation gradient, the Cauchy stress \mathbf{T} can be related to the deformation by

$$\mathbf{T} = J^{-1} \mathbf{F} \cdot \frac{\partial W}{\partial \mathbf{F}} - p \mathbf{I}, \quad (13)$$

where p is as previously defined and J is the determinant of \mathbf{F} .

We introduce a Lagrangian measure of the stress, specifically the first Piola-Kirchoff stress tensor \mathbf{P} given by

$$\mathbf{P} = J \mathbf{T} \mathbf{F}^{-T}, \quad (14)$$

which relates forces with respect to the current configuration to those with respect to the reference configuration. The reference configuration is defined to be the configuration of the layers when no external force is applied, and the coordinates of the reference configuration are defined as the Cartesian coordinates (X, Y, Z) .

The equation for the balance of linear momentum in terms of \mathbf{P} is

$$\text{Div} \mathbf{P} = 0, \quad (15)$$

where the operator Div is the divergence with respect to the reference configuration.

Now, in order to produce a tractable model, we make the following assumptions. First, we consider the two-dimensional problem, i.e. we consider that all dependent variables are independent of Y . Second, we assume incompressibility, in which case we have $J = 1$. We also will ignore the contact problem of the indenter with the material. Finally, we consider a simplification of the material model. From the previous section, we know we must consider a nonlinear model. As a first consideration, we will assume a neo-Hookean material model, which may be considered as a weakly nonlinear version of the exponential model of Equation (1). In particular, we consider the strain energy density function $W = C(I_1 - 2)$, where C is a material constant and I_1 is as in Equation (1). Below, we will see that this

model is not able to reproduce the force-deformation data of the experiments. However, the assumption provides significant simplification, while it is still expected to provide a reasonable first approximation.

With these assumptions, in the case where there is a single layer, Equation (15) becomes

$$\frac{\partial P_{XX}}{\partial X} + \frac{\partial P_{XZ}}{\partial Z} = 0, \quad (16a)$$

$$\frac{\partial P_{ZX}}{\partial X} + \frac{\partial P_{ZZ}}{\partial Z} = 0, \quad (16b)$$

$$u_X + w_Z + u_X w_Z - u_Z w_X = 0, \quad (16c)$$

where $\mathbf{u} = (u, w)$ is the displacement vector and

$$P_{XX} = [2C((1+u_X)^2 + u_Z^2) - p](1+w_Z) - 2C[(1+u_X)w_X + u_Z(1+w_Z)]u_Z, \quad (17a)$$

$$P_{XZ} = -[2C((1+u_X)^2 + u_Z^2) - p]w_X + 2C[(1+u_X)w_X + u_Z(1+w_Z)](1+u_X), \quad (17b)$$

$$P_{ZX} = 2C[(1+u_X)w_X + u_Z(1+w_Z)](1+w_Z) - [2C(w_X^2 + (1+w_Z)^2) - p]u_Z, \quad (17c)$$

$$P_{ZZ} = -2C[(1+u_X)w_X + u_Z(1+w_Z)]w_X + [2C(w_X^2 + (1+w_Z)^2) - p](1+u_X). \quad (17d)$$

The boundary conditions around the outer walls of the rectangular geometry are

$$u = 0, \quad w = 0, \quad \text{on } Z = 0, \quad (18a)$$

$$P_{XX} = 0, \quad P_{ZX} = 0, \quad \text{on } X = \pm 1, \quad (18b)$$

$$P_{XZ} = 0, \quad P_{ZZ} = \tau \delta(x), \quad \text{on } Z = h. \quad (18c)$$

For the case of a two-layered model, Equations (16)–(18) hold in each layer and we use the notation $u^{(i)}, w^{(i)}, p^{(i)}, i = 1, 2$ to denote u, w and p evaluated in the lower and upper layers, respectively. At the interface of the two layers, $Z = h_1$, the associated tractions need to be equal but opposite, which requires the stress to be continuous across Z , and the vertical displacement must be equal, thus

$$P_{ZZ}^{(1)} = P_{ZZ}^{(2)}, \quad w^{(1)} = w^{(2)} \quad \text{on } Z = h_1, \quad (19)$$

where $Z = h_1$ is the interface of the layers in the initial configuration.

1.5 Numerical simulations

Finite element simulations were performed using the commercial software ANSYS (ANSYS, Inc., Canonsburg, PA, USA). The leaflet-indenter system was modelled using a two-dimensional axisymmetric geometry. The indenter was modelled as a rectangle with a filleted bottom corner. This filleted corner mimics the actual indenter, which has slightly rounded edges. Layer heights, which were either arbitrarily defined or based on calculations made from segmented ultrasound images, were assumed to be constant over the simulation geometry, and the width of

the leaflet geometry was assumed to be sufficiently large to make edge effects negligible, but not too large as to increase the computational time for the simulations unnecessarily. The indenter was meshed using 6-node triangular elements, while the leaflet layers were meshed using 8-node quadrilateral elements, with elements concentrated near the indenter and at the interfaces between layers. An example of the model geometry and mesh is shown in Figure 8.

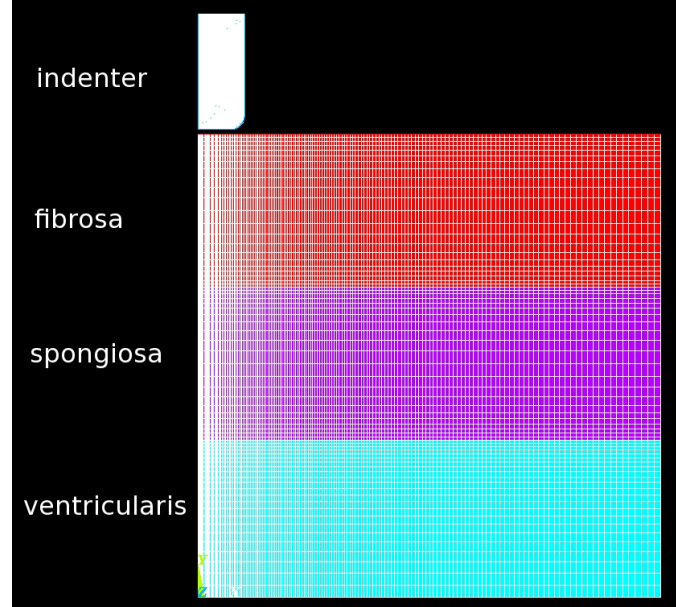


Figure 8. Leaflet-indenter system geometry and mesh

Indentation depths, either representative values or values from measurements, were applied as input boundary conditions to the top edge of the indenter. The left edges of the geometry are axisymmetric boundaries, and the right edges are free boundaries. There is no slip between the layers, and no displacement on the bottom. Contact boundary conditions, defined through the use of contact and target elements in ANSYS, were applied to the top edge of the leaflet and the bottom, curved and right edges of the indenter.

Large displacement static simulations of the leaflet indentation were performed. The indenter was assumed to be a linear elastic material with $E = 2 \times 10^8$ kPa and $\nu = 0.49$. Each leaflet layer was assumed to be slightly compressible (to allow for numerical convergence), isotropic, and homogenous over the simulated geometry. Initial simulations were performed using a neo-Hookean material model, defined as

$$W = C(\bar{I}_1 - 3) + \frac{1}{d}(J - 1)^2, \quad (20)$$

where \bar{I}_1 is the first deviatoric strain invariant, d is the incompressibility parameter, and J is the determinant of the deformation gradient tensor \mathbf{F} .

It has previously been shown [10] that if the incompressibility parameter d is selected sufficiently small, the compressibility effects in the slightly compressible form of a hyperelastic material

model become negligible and the results for the slightly compressible material model converge to those for the equivalent incompressible material model. Therefore, material parameter values calculated from mathematical models that use the incompressible form of W are equivalent to values used in simulations performed with the slightly compressible form of the same W .

1.6 Nonlinear optimization

To determine the material parameter values for each leaflet layer from the measured data, an inverse finite element approach was used in conjunction with nonlinear optimization in MATLAB. The finite element model has been written in a text-based input format that allows for straightforward modifications to the input parameters. By defining the finite element model in this manner, it allowed the finite element simulations to be modified and run from within MATLAB. The sequence of steps is as follows:

1. Input values for indentation depths, layer heights, and material model parameters are defined either arbitrarily or from measured data and mathematical models.
2. ANSYS input file automatically modified with these values.
3. Finite element simulations performed and indentation force versus indentation depth data is output.
4. Indentation force versus indentation depth data is imported into MATLAB and the least squares error is calculated between the input and output data from the finite element simulations.
5. If the least squares error is less than a threshold, then the simulations are complete and the material parameter values are determined. If the results have not converged, non-linear optimization, using the `fmincon` function in MATLAB, is used to calculate new material model parameter values. The simulations are repeated in this manner until convergence has been reached.

2. Results and Discussion

2.1 Mathematical models

For the two-layer one-dimensional problem, described in Section 1.4.3, we have performed numerical tests for the linear and cubic nonlinear cases. For these tests, we have assumed the bottom layer (1) to have linear material properties and the top layer (2) to have nonlinear properties. Note that as in Section 1.4.3, the subscripts in this section represent the different layers. For the linear case, we have $F = \tilde{C}_1 \delta_1 = \tilde{C}_2 \delta_2$ and $h_1 \delta_1 + h_2 \delta_2 = -U$, where $\tilde{C}_1 = C_{11}C_{12}$ and $\tilde{C}_2 = C_{21}C_{22}(1 + 2C_{22})$. These two relationships lead to

$$\frac{h_1}{\tilde{C}_1} + \frac{h_2}{\tilde{C}_2} = -\frac{F}{U}. \quad (21)$$

Therefore, taking multiple measurements does not help to find \tilde{C}_1 and \tilde{C}_2 , and the solution is not unique.

For the nonlinear case, however, things are different. We consider the simplest possible case with a combination of a linear elastic layer with a cubic nonlinear elastic layer, $F =$

$\tilde{C}_1 \delta_1 = \tilde{C}_2 \delta_2^3$ and $h_1 \delta_1 + h_2 \delta_2 = -U$. In this case, we have

$$\frac{1}{\tilde{C}_1} h_1 F + \frac{1}{\tilde{C}_2^{1/3}} h_2 F^{1/3} = -U. \quad (22)$$

We can solve for \tilde{C}_1 and \tilde{C}_2 using a least squares approach with multiple measurements $F(k)$ and $U(k)$ by solving the following over-determined linear system

$$A\mathbf{x} = \mathbf{y} \quad (23)$$

where the i -th row of A and \mathbf{y} are given by

$$A_i = [h_1 F(i); h_2 F^{1/3}(i)], \quad y_i = -U(i), \quad (24)$$

with two unknowns $x_1 = 1/\tilde{C}_1$ and $x_2 = 1/\tilde{C}_2^{1/3}$. In Figure 9, we have the force-indentation depth curve for $\tilde{C}_1 = 1$ and $\tilde{C}_2 = 50$ without, and with, a normally distributed random measurement error. The material parameter values are estimated as $\tilde{C}_1 = 1$ and $\tilde{C}_2 = 50$ (without noise) and $\tilde{C}_1 = 0.983$ and $\tilde{C}_2 = 56.20$ (with noise, $\sigma = 0.015$).

Remark. Note that for the more general nonlinear elasticity $F = C'_1(\delta + C'_2\delta^3)$, the procedure is almost the same except that we need to solve a cubic equation for δ before setting up the least squares problem. For the more general exponential elasticity $R(\lambda) \exp(C_2 S(\lambda))$, however, a numerical method is needed.

Work is ongoing to extend the one-dimensional models to three layers and to incorporate nonlinear material properties in all of these layers. A tailor-made solver is being developed to study the two-dimensional nonlinear problem. This solver will initially look at the two layer problem and then will be extended to three layers.

2.2 Numerical simulations

Numerical simulations of the forward problem have been successfully performed with arbitrary indentation depths, layer heights, and material parameter values, using the neo-Hookean material model. Figures 10 and 11 are contour plots of the resulting nodal displacements and von Mises stresses, respectively. These results show the feasibility of performing the finite element simulations of this indentation problem.

The neo-Hookean material model (Equation 20) was chosen for initial simulations, because it only has one unknown and is already implemented in ANSYS. However, the resulting stress-indentation curves (Figure 12) did not have the same trend as the indentation force-depth measurements. More specifically, the numerical results show a nearly linear stress-indentation depth relationship, while the measured indentation force-depth curves had exponential forms. The next step is to perform the simulations with the exponential hyperelastic material model (Equation 1), which is not implemented in ANSYS and requires a user-defined function. Work on this user-defined function is ongoing, and subsequent simulations will be performed using

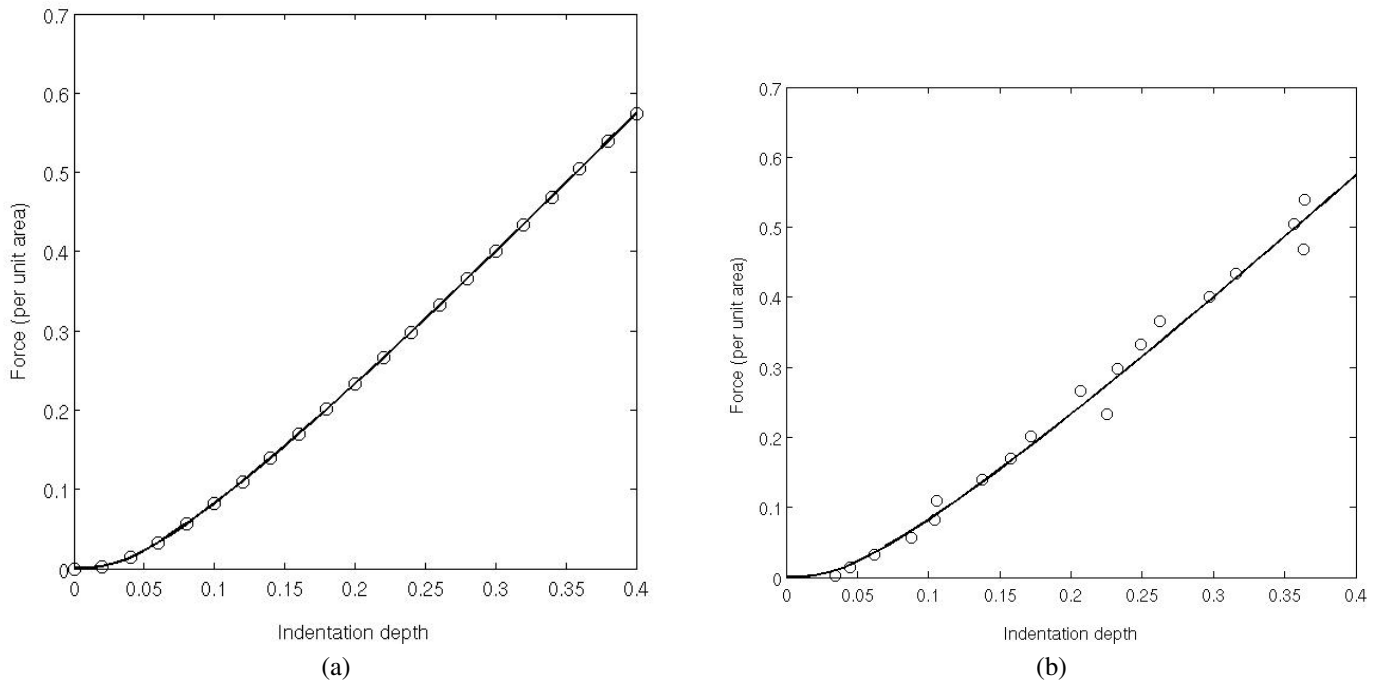


Figure 9. Force-indentation depth curve for the linear-cubic test case with $\tilde{C}_1 = 1$ and $\tilde{C}_2 = 50$: (a) without measurement noise and (b) with normally distributed measurement noise with $\sigma = 0.015$.

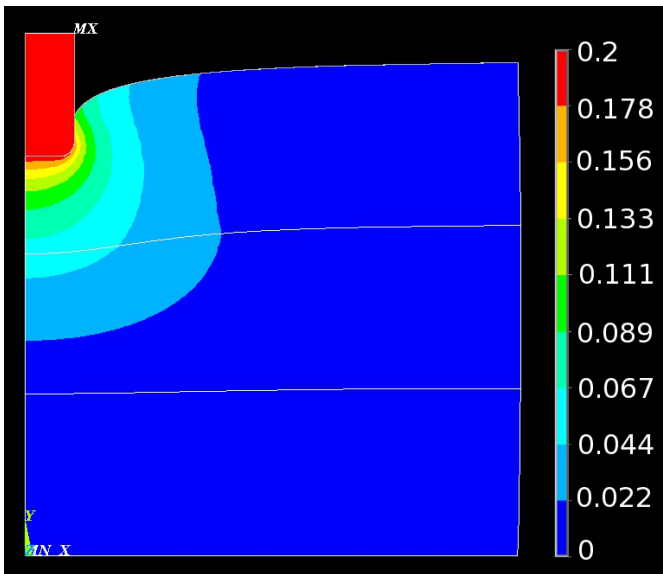


Figure 10. Contour plot of nodal displacements (in mm)

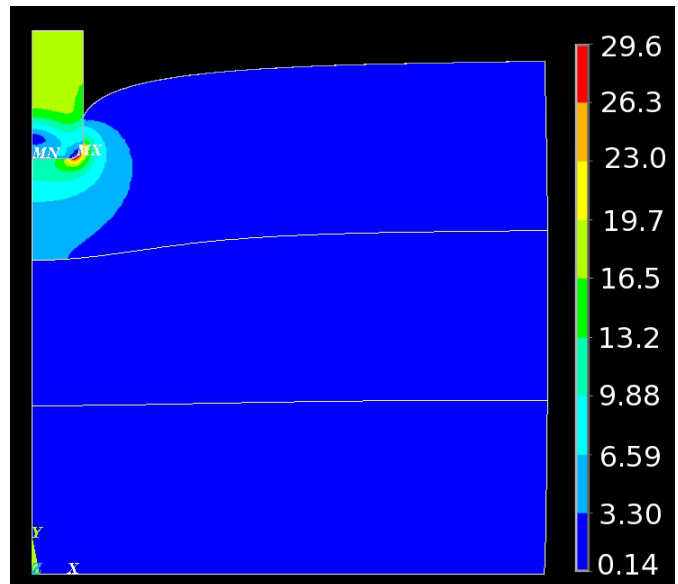


Figure 11. Contour plot of von Mises stresses (in kPa)

the slightly compressible version of Equation (1), which is defined as

$$W = \frac{C_1}{2} \left(e^{C_2(\bar{I}_1-3)} - 1 \right) + \frac{1}{d}(J-1)^2, \quad (25)$$

2.3 Nonlinear optimization

Steps 1-3 of the sequence defined in Section 1.6 have been successfully implemented. That is, the finite element simulations can be run and modified from within MATLAB. These simulations have so far been run using representative data. Upon implementation of the user-defined material model based on Equation (25) in ANSYS, specimen-specific simulations will be

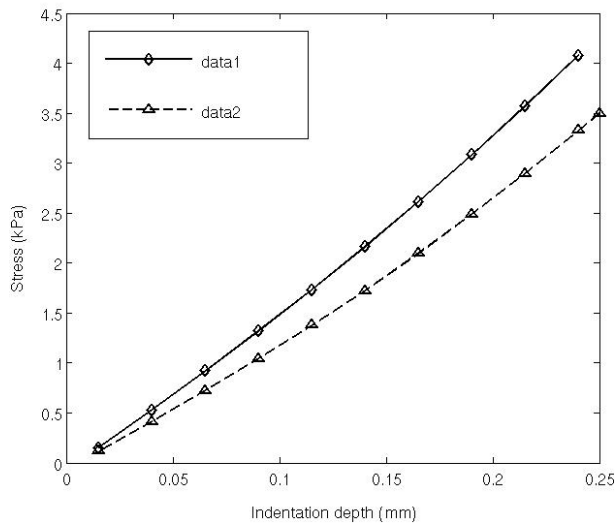


Figure 12. Stress-indentation depth curves from simulations with the neo-Hookean material model

performed using the previously described sequence of steps. At this point, the nonlinear optimization function will be added to the workflow so that material parameter values can be calculated from the experimental data.

3. Conclusions

A combined experimental and computational method has been proposed for determining the microscale mechanical properties of each of the three layers of porcine aortic valve leaflets. A microindenter has been built to measure indentation force and depth, and image processing tools have been developed to calculate leaflet layer heights from ultrasound images. Mathematical models have been developed for one-dimensional problems for one and two layer models. Numerical examples have been presented to illustrate the two cases for a two-layer one-dimensional problem, linear, which does not lead to a unique solution for the material parameters, and cubic nonlinear, which does lead to a unique solution for the material parameters assuming sufficient data points are available. A numerical method for two-dimensional problems has been proposed and a custom solver is currently being developed for this problem. Finite element simulations of the leaflet-indenter system have been performed for a simple hyperelastic material model and work is presently underway to implement the proposed exponential hyperelastic material model in ANSYS and repeat the simulations with this model. Upon completion of these simulations, specimen-specific simulations will be performed coupled with non-linear optimization to calculate the material parameter values for each of the leaflet layers.

Acknowledgments

We are grateful to the organizers of the MBI Biosciences Problem Solving Workshop in July 2012 for putting on the event that inspired the work presented in this paper. Funding was provided

by the Natural Sciences and Engineering Research Council of Canada (NSERC), a Fields-Centre for Mathematical Medicine Postdoctoral Fellowship (M.G.D), a Heart and Stroke/Richard Lewar Centre of Excellence Fellowship (M.G.D), and the Canada Research Chair in Mechanobiology (C.A.S).

References

- [1] B. F. Stewart, D. Siscovick, B. K. Lind, J. M. Gardin, J. S. Gottdiener, V. E. Smith, D. W. Kitzman, and C. M. Otto. Clinical factors associated with calcific aortic valve disease. *J. Am. Coll. Cardiol.*, 29:630–634, 1997.
- [2] C. Y. Yip, J. H. Chen, R. Zhao, and C. A. Simmons. Calcification by valve interstitial cells is regulated by the stiffness of the extracellular matrix. *Arterioscler. Thromb. Vasc. Biol.*, 29:936–942, 2009.
- [3] J.H. Chen, W. L. K. Chen, K. L. Sider, C. Y. Y. Yip, and C. A. Simmons. β -catenin mediates mechanically regulated, transforming growth factor- β 1 induced myofibroblast differentiation of aortic valve interstitial cells. *Arterioscler. Thromb. Vasc. Biol.*, 31:590–597, 2011.
- [4] K. L. Sider, M. C. Blaser, and C. A. Simmons. Animal models of calcific aortic valve disease. *Int. J. Inflamm.*, 2011:1–18, 2011.
- [5] M.-K. Sewell-Loftin, C. B. Brown, H. S. Baldwin, and W. D. Merryman. A novel technique for quantifying mouse heart valve leaflet stiffness with atomic force microscopy. *J. Heart Valve Dis.*, 21:513–520, 2012.
- [6] R. Zhao, K. L. Sider, and C. A. Simmons. Measurement of layer-specific mechanical properties in multilayered biomaterials by micropipette aspiration. *Acta Biomater.*, 7:1220–1227, 2011.
- [7] M. G. Doyle, C. A. Simmons, C. Breward, H. Byrne, P.-W. Fok, H. Huang, G. Lewis, D. Moulton, S. O’Keefe, D. Schwendeman, S. Sivaloganathan, J. Siggers, T. Stepien, Y.-H. Tseng, and R. Vandiver. Microindentation of aortic valve leaflet local micromechanical properties. In *Proceedings of the MBI BioSciences Problem-Solving Workshop*, pages 1–10, 2012.
- [8] Q. Qiu, J. Dunmore-Buyze, D. R. Boughner, and J. C. Lacefield. Evaluation of an algorithm for semiautomated segmentation of thin tissue layers in high-frequency ultrasound images. *IEEE Trans. Ultrason., Ferroelectr., Freq. Control*, 53:324–334, 2006.
- [9] T. P. Usyk and A. McCulloch. Computational methods for soft tissue biomechanics. In G. Holzapfel and R. W. Ogden, editors, *Biomechanics of soft tissue in cardiovascular systems*, pages 273–341, 2003.
- [10] M. G. Doyle, S. Tavoularis, and Y. Bourgault. Adaptation of a rabbit myocardium material model for use in a canine left ventricle simulation study. *J. Biomech. Eng.*, 132:041006–01–041006–12, 2010.